ACS OMEGA

Article

Cite This: ACS Omega 2018, 3, 17814−17820

http://pubs.acs.org/journal/acsodf

Facile Synthesis and Controllable Emission of Tm^{3+}/Er^{3+}-Doped and -Co-doped α-$NaYbF_4$ Upconversion Nanocrystals

Huilin He,[†,§] Ying Zhang,[†] Yong Li,[†] Lihong Wang,[†] Xian Gao,[†] Xi Zhang,[‡] Danqiong He,[‡] Rui Chen,[†] Dan Luo,[†] Xiao Wei Sun,[†,∥] and Yan Jun Liu*[,†,∥]

[†]Department of Electrical and Electronic Engineering and [‡]Department of Biomedical Engineering, Southern University of Science and Technology, Shenzhen 518055, China

[§]Harbin Institute of Technology, Harbin 150001, China

[∥]Shenzhen Planck Innovation Technologies Pte Ltd, Ganli 6th Road, Longgang, Shenzhen 518112, China

ABSTRACT: Tm^{3+}, Er^{3+}-doped and -co-doped α-$NaYbF_4$ nanoparticles were synthesized via a facile hydrothermal route with oleic acid as the capping agent. Experimental results showed that the doped $NaYbF_4$ nanoparticles possessed a cubic phase with the average size of ∼13 nm. Upon excitation by a 980 nm laser, the as-synthesized nanoparticles exhibited blue and red upconversion emissions corresponding to the monodoped Tm^{3+}, Er^{3+} in the cubic-phase $NaYbF_4$, respectively, and intense green and red emissions in the Tm^{3+}/Er^{3+}-co-doped $NaYbF_4$ nanoparticles. Furthermore, the possible energy transfer mechanism among $Yb^{3+}/Tm^{3+}/Er^{3+}$ in α-$NaYbF_4$ nanoparticles was also proposed. The cell toxicity test revealed that the as-synthesized upconversion nanoparticles possessed remarkably low cytotoxicity. All of the advantageous features including facile synthesis, controllable emission, and low cytotoxicity make the upconversion nanoparticles promising for multicolor bioimaging and anti-counterfeiting applications.

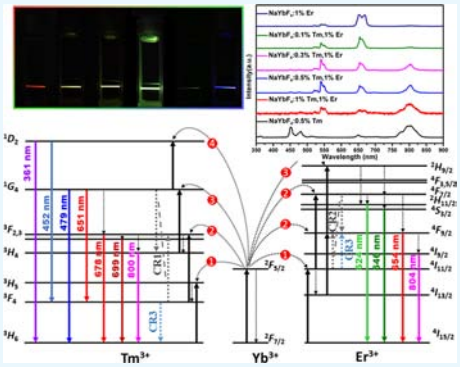

1. INTRODUCTION

Over the past decade, the upconversion nanoparticles (UCNPs) with lanthanide doping, converting low-energy excitation light [e.g., the NIR or IR] into high-energy emission (e.g., ultraviolet, visible, or NIR), have shown a wide range of potential applications in lighting and displays, bioimaging, therapeutics, and photovoltaic devices because of their excellent photostability, large anti-Stokes shift, narrow-band emission, and long excited-state lifetime.[1−6] Among the lanthanide ions, the Yb^{3+} ion has attracted great attention for decades owing to its high absorption cross section at the excitation wavelength of ∼980 nm, which also lies in the NIR optical window for biological tissues. Moreover, Yb^{3+} ions are also an effective sensitizer to transfer the absorbed photon energy to the nearby activators to yield efficient upconversion luminescence (UCL).[1−6] So far, most studied co-doping or tridoping systems have a relatively lower Yb^{3+} doping level (typically less than 20%) for the reason of UCL quenching, especially in the short wavelength range.[7−10] However, some unique UCL properties in the high-level Yb^{3+} ion doping environment have also aroused much attention in recent years. For instance, Chen et al.[11] reported that the intensity of NIR UCL can be increased by up to 43 times when they increased the relative content of Yb^{3+} ions up to 100% in $NaYF_4$:Yb^{3+}, Tm^{3+} nanocrystals. They also demonstrated the core/shell (α-$NaYbF_4$:Tm^{3+})/CaF_2 nanoparticles that exhibit highly efficient NIR_{in}−NIR_{out} UCL for high-contrast deep tissue bioimaging.[12] In addition, Liu group has also found an intense four-photon-promoted violet UCL in KYb_2F_7:Er^{3+} nanocrystals.[8] As a result, Yb^{3+} ions could play two major roles as both a host matrix and an excellent sensitizer to improve the UCL performance in the high-level Yb^{3+} ion doping environment, and achieve the particular emission properties in upconversion nanomaterials.

In the upconversion emission systems, energy transfer (ET) is the major mechanism to achieve the desired emission with high UCL efficiency.[6,13] Especially, Yb^{3+} ions act as an effective sensitizer to transfer the absorbed photon energy to some typical activators (e.g., Tm^{3+}, Er^{3+}, and Ho^{3+} ions) and then generate the corresponding multicolor emissions. Among the NIR-triggered upconversion systems, the multicolor outputs (blue, green, and red emissions) can be controllably tuned via co-doping Yb^{3+}/Tm^{3+}, Yb^{3+}/Ho^{3+}, and Yb^{3+}/Er^{3+} pairs.[14−16] In addition, researchers have even reported the generation of multicolor and white-light emissions with more complex systems including the tridoping system for the diversity of UCL emissions, such as $Yb^{3+}/Tm^{3+}/Ho^{3+}$ in β-$NaLuF_4$ microstructures[16] and $Yb^{3+}/Tm^{3+}/Er^{3+}$ in Lu_2O_3 nanocrystals.[17] However, in the complex multidoping systems, there exist many nonradiative transition channels, exerting a negative effect on the UCL efficiency. Thus, the controllable synthesis of high-quality UCNPs and the ET-modulated UCL have

Received: October 25, 2018
Accepted: December 6, 2018
Published: December 19, 2018

DOI: 10.1021/acsomega.8b02936
ACS Omega 2018, 3, 17814−17820

become extremely critical because of the high demand for multicolor UCL in bioimaging, security, and anticounterfeiting applications.[4,6,15,18−20] It is worth noting that $NaYbF_4$, as a host, could also play an important role in minimizing the excessive nonradiative transition in the multidoping systems. Nevertheless, studies on the controllable UCL emission and energy transfer of Tm^{3+}/Er^{3+} pairs in the $NaYbF_4$ UCNPs still remain insufficient.

Therefore, in this work, we report a facile hydrothermal method to synthesize the Tm^{3+}/Er^{3+}-doped and -co-doped α-$NaYbF_4$ UCNPs. The morphologies and phase of as-synthesized UCNPs are studied in detail. In a high Yb^{3+} ion doping environment, the UCNPs exhibit the blue and red UCL corresponding to the monodoped Tm^{3+}, Er^{3+} in the α-$NaYbF_4$ under excitation of a 980 nm laser, respectively. For the Tm^{3+} co-doping in $NaYbF_4$:Er^{3+} UCNPs, intense green UCL is observed because of the cross relaxation between Tm^{3+}/Er^{3+}. The possible ET mechanism among $Yb^{3+}/Tm^{3+}/Er^{3+}$ in α-$NaYbF_4$ UCNPs has been proposed on the basis of the plots of UCL intensity versus power density and the lifetime decay curves. The cell toxicity test shows that the as-synthesized $NaYbF_4$ UCNPs possess remarkably low cytotoxicity. The achieved results indicate that $NaYbF_4$ UCNPs with multicolor emission may have a huge potential for bioimaging and anticounterfeiting applications.

2. RESULTS AND DISCUSSION

2.1. Controllable Synthesis of Tm^{3+}/Er^{3+}-Doped $NaYbF_4$ Nanocrystals. To check the crystalline phase of the as-synthesized sample, Figure 1 shows the X-ray diffraction (XRD) patterns of different dopants in $NaYbF_4$. It can be clearly seen from Figure 1 that all of the diffraction peaks in the patterns can be indexed to the standard card of $NaYbF_4$ (JCPDS #77-2043) with the lattice constants of $a = b = c = 5.471$ Å, $\alpha = \beta = \gamma = 90°$. No other impurity phases were detected, which indicates that the as-synthesized products are purely cubic phase. With the diverse doping concentrations of Er^{3+} and Tm^{3+} ions, the crystalline structure of $NaYbF_4$ remained the same, meaning that the low-concentration Er^{3+} and Tm^{3+} ions have negligible influence on the $NaYbF_4$ crystal structure.

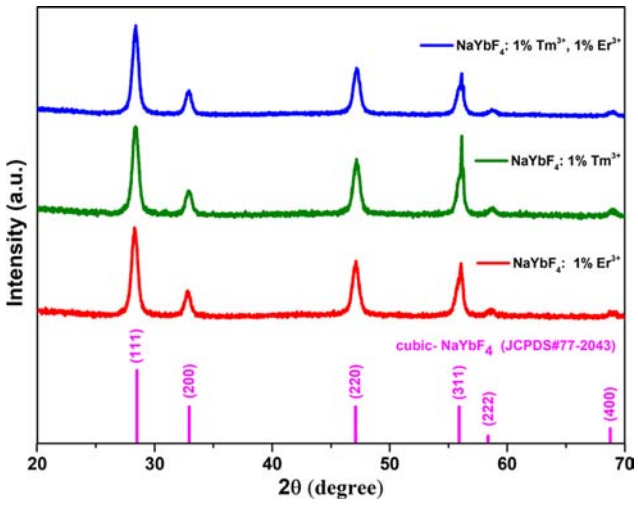

Figure 1. XRD pattern of as-synthesized $NaYbF_4$ nanocrystals with different dopants.

The morphologies, compositions, and crystal structures of as-synthesized doped $NaYbF_4$ nanocrystals were also characterized by transmission electron microscopy (TEM) and high-resolution TEM (HRTEM). Figure 2 shows the typical results by taking $NaYbF_4$:1%Tm^{3+} nanocrystals as an example. Figure 2a exhibits the TEM image of the synthesized product that consists of a series of nanoparticles with the size ranging from 6 to 21 nm [see Figure 2c]. The HRTEM image [Figure 2b] reveals that the clear crystal lattice fringes with the *d*-spacing values of 0.2718 and 0.3084 nm correspond to (200) and (111) *d*-spacing of the cubic-phase $NaYbF_4$ (α-$NaYbF_4$ phase), respectively. Moreover, energy-dispersive spectroscopy (EDS) of the corresponding product clearly shows the peaks according to the designed elements (Na, Yb, Tm, and F) in Figure 2d. Furthermore, Figure 2e−i shows the two-dimensional mapping distribution of Na, Yb, Tm, and F elements, showing a very uniform distribution in a single α-$NaYbF_4$ nanocrystal. Therefore, we can confirm from the results in Figure 2e−i that the product is mainly composed of Na, Yb, Tm, and F elements, and Tm is evenly distributed in the cubic $NaYbF_4$ matrix nanocrystals.

2.2. UCL Properties and ET Mechanism. Subsequently, UCL properties of the as-synthesized doped $NaYbF_4$ nanocrystals have been investigated upon excitation by a 980 nm laser. The UCL spectra of as-synthesized $NaYbF_4$:0.5%Tm^{3+}, $NaYbF_4$:1%Er^{3+} nanocrystals are shown in Figure 3, which displays the characteristic emission peaks of Tm^{3+} (blue curve) and Er^{3+} (red curve) ions. The blue curve in Figure 3 describes the following transitions of Tm^{3+} ions. For the visible region: $^1D_2 \rightarrow {}^3H_6$ (361 nm), $^1D_2 \rightarrow {}^3F_4$ (452 nm), $^1G_4 \rightarrow {}^3H_6$ (479 nm), $^1G_4 \rightarrow {}^3F_4$ (651 nm), $^3F_2 \rightarrow {}^3H_6$ (678 nm), and $^3F_3 \rightarrow {}^3H_6$ (699 nm), and for the NIR region: $^3H_4 \rightarrow {}^3H_6$ (800 nm). In addition, the inset (left side) shows the eye-visible blue emission in the synthesized $NaYbF_4$:0.5%Tm^{3+} colloidal suspension because of the UCL band from 435 to 550 nm, though the emission peak at 800 nm (invisible region) is the strongest one, which may be ascribed to the effective absorption of high concentration of Yb^{3+} ions and increased ET efficiencies between Yb^{3+} and Tm^{3+} in the $NaYbF_4$ nanocrystal.[11] On the other hand, the red curve in Figure 3 shows the spectral peaks of Er^{3+} corresponding to the following transitions: $^2H_{11/2} \rightarrow {}^4I_{15/2}$ (524 nm), $^4S_{3/2} \rightarrow {}^4I_{15/2}$ (546 nm), $^4F_{9/2} \rightarrow {}^4I_{15/2}$ (654 nm), and $^4I_{9/2} \rightarrow {}^4I_{15/2}$ (804 nm). The inset (right side) shows the eye-visible red emission in the synthesized $NaYbF_4$:1%Er^{3+} colloidal suspension, which is ascribed to the red UCL (654 nm) intensity dominated in the visible range when excited by a 980 nm laser.

To reveal the ET mechanism of the upconversion emission involved in the Er^{3+} and Tm^{3+} ions in the cubic $NaYbF_4$ nanocrystals, the dependence of the UCL intensity on the pump-laser power density has been investigated in detail as shown in Figure 4a,b. In principle, the UCL intensity has a power dependence on the NIR excitation laser power over a limited range, which can be written as $I_{UC} \propto (I_{NIR})^n$, where n is the number of absorbed photons during the process.[21,22] Experimentally, the n value is the slope of corresponding fitted lines, as shown in Figure 4c,d. For the emission spectrum of Tm^{3+} ions in the visible range (361, 452, 479, 651, and 699 nm) and the NIR range (800 nm), the corresponding n values in Figure 4c are 3.40, 3.35, 2.11, 2.42, 1.53, and 1.55. In this way, the respective emission can be then categorized according to the number of photons (n value) absorbed in that particular

DOI: 10.1021/acsomega.8b02936
ACS Omega 2018, 3, 17814−17820

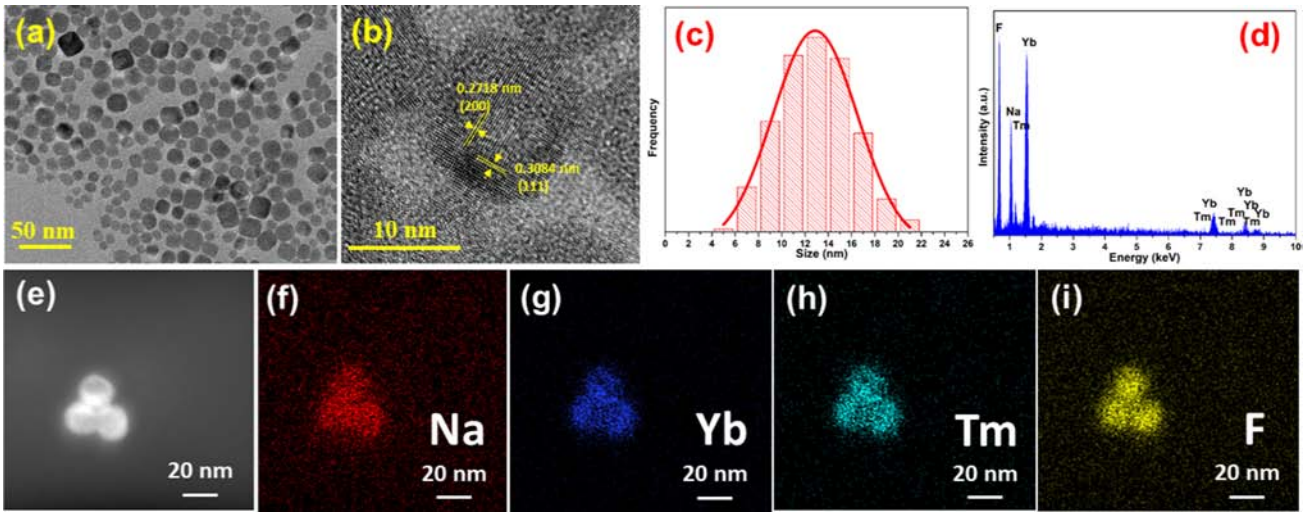

Figure 2. (a–d) TEM image, HRTEM image, size distribution, and EDS spectrum of as-synthesized Tm^{3+}-doped $NaYbF_4$ nanocrystals, respectively. (e–i) Two-dimensional mapping distribution of Na, Yb, Tm, and F, respectively.

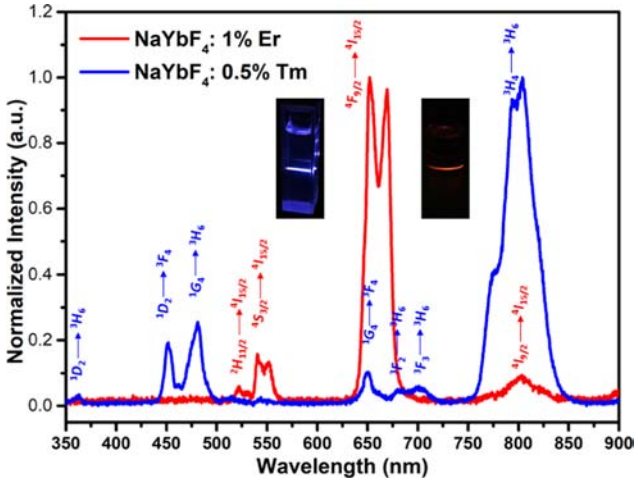

Figure 3. Room-temperature upconversion emission spectra of as-synthesized $NaYbF_4$:1%Er^{3+} (red curve) and $NaYbF_4$:0.5%Tm^{3+} (blue curve) under excitation of a 980 nm laser. (The left and right insets show the visible photoluminescence images of the $NaYbF_4$:0.5%Tm^{3+} and $NaYbF_4$:1%Er^{3+} UCNP colloidal suspensions excited by the 980 nm laser, respectively.)

UC process: four-photon (361 and 452 nm), three-photon (479 and 651 nm), and two-photon (699 and 800 nm) processes. On the basis of the analysis above, the ET mechanism of UCL can be illustrated as shown in Figure 5, which exhibits schematic energy-level diagrams of Yb^{3+}, Tm^{3+}, and Er^{3+} ions. Upon the NIR laser irradiation, the Yb^{3+} ions are excited to the $^2F_{5/2}$ state from the ground state $^2F_{7/2}$, and then transfer the energy to Tm^{3+} ions. In principle, the $^1G_4$ state of Tm^{3+} can be easily populated by a Yb-assisted three-photon ET process, and then continue to accept energy to transit to an even higher excited-state $^1D_2$ state (four-photon process). However, a cross-relaxation (CR1) process of $^1G_4$ (Tm^{3+}) + $^3F_4$ (Tm^{3+}) → $^3H_4$ (Tm^{3+}) + $^3F_2$ (Tm^{3+}) between Tm^{3+} ions may play a vital role in depopulating the $^1G_4$ state, and facilitate the photon population of $^3H_4$, which can further explain the intense NIR UC emission (800 nm) in the whole UCL spectrum. In addition, the higher-concentration Yb^{3+} ions also prefer the four-photon process (452 nm), especially under the higher excitation power density in Figure 4a.[10] Meanwhile, for the visible (524, 546, 654, and 667 nm) and NIR (804 nm) UCL of Er^{3+} ions, the corresponding n values in Figure 4d are 2.11, 1.93, 1.83, 1.85, and 1.43, which indicates that the 524 nm UCL may involve a three-photon process and the others (546, 654, 667, and 804 nm) are two-photon processes. The corresponding ET mechanism from Yb^{3+} ions to Er^{3+} ions is also depicted in Figure 5. Via a Yb-assisted two-photon ET process, the Er^{3+} ions can be promoted to the $^4F_{7/2}$ and $^4F_{9/2}$ states. As demonstrated above, the UCL of Er^{3+} ions prefer to give out red UC emission (654 nm) in the α-$NaYbF_4$ nanocrystal, which may be due to the CR2 process: $^4F_{7/2}$ (Er^{3+}) + $^4I_{11/2}$ (Er^{3+}) → $^4F_{9/2}$ (Er^{3+}) + $^4F_{9/2}$ (Er^{3+}) of adjacent Er^{3+} ions in a α-$NaYbF_4$ nanocrystal with a high-concentration Yb^{3+} ion environment, thus facilitating the population at $^4F_{9/2}$ state, and a high red/green (R/G emission) ratio in the $NaYbF_4$:1%Er^{3+}.

Moreover, with different Tm^{3+} doping concentrations, the Tm^{3+} and Er^{3+} ion co-doping in the cubic $NaYbF_4$ nanocrystals has also been studied in this work. Figure 6a shows the UCL spectra of as-synthesized $NaYbF_4$ nanocrystals with different dopants and concentrations under the NIR laser excitation. It can be clearly observed from the spectra that the green UCL ($^4S_{3/2}$ → $^4I_{15/2}$, 544 nm) of Er^{3+} ion in the α-$NaYbF_4$ nanocrystals can be greatly enhanced with co-doping of Tm^{3+} ions, whereas the short-wavelength UCL ($^1D_2$ → $^3H_6$ (361 nm), $^1D_2$ → $^3F_4$ (452 nm), and $^1G_4$ → $^3H_6$, (477 nm)) of Tm^{3+} ions quenches in the meantime. In addition, the red and green UCL ratio (R/G ratio) in the Er^{3+}:$NaYbF_4$ samples with or without Tm^{3+} co-doping has also been calculated in Figure 6b; it is obvious that the R/G ratio in these samples decreases with the increasing co-doping Tm^{3+} concentration from 0 to 1%. Thus, with the Tm^{3+} and Er^{3+} ion co-doping, strong eye-visible green-yellow UCL can be achieved in the synthesized α-$NaYbF_4$ nanocrystal colloidal suspension, as shown in the inset of Figure 6b.

To understand the ET mechanism of the UCL involved in the Yb^{3+}, Tm^{3+}, and Er^{3+} ions in the cubic $NaYbF_4$ nanocrystals, Figure 7a,b shows the dependence of the UCL intensity on the pump-laser power density in detail. For the typical UCL of a Tm^{3+} ion (477, 697, and 804 nm), the corresponding n values in Figure 7a are 2.83, 1.56, and 1.76,

DOI: 10.1021/acsomega.8b02936
ACS Omega 2018, 3, 17814–17820

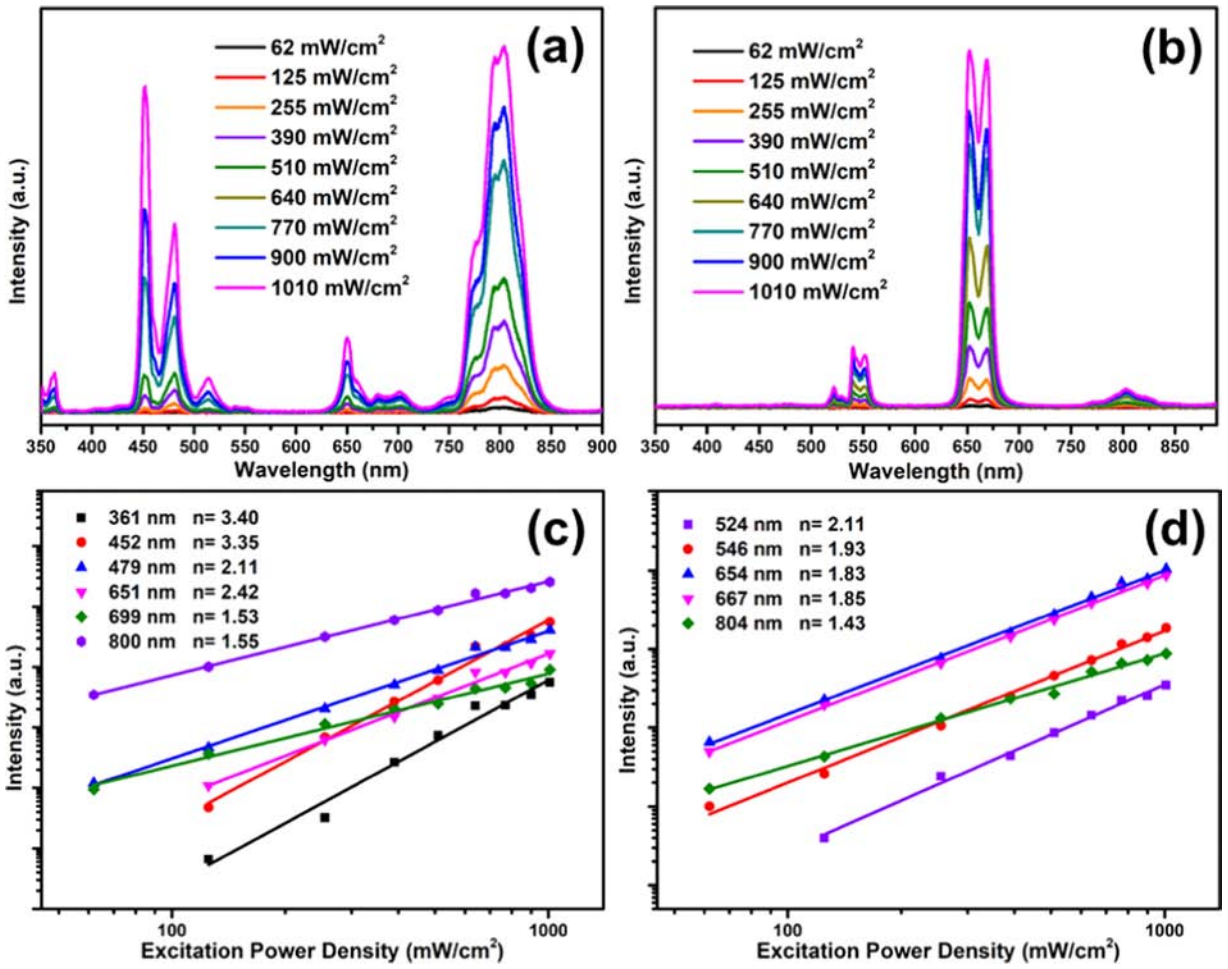

Figure 4. (a, b) UCL intensities at different excitation power intensities of as-synthesized $NaYbF_4$:0.5%Tm^{3+} and $NaYbF_4$:1%Er^{3+}. (c, d) Corresponding excitation power densities' dependence on the emission of UCNPs under excitation of a 980 nm laser.

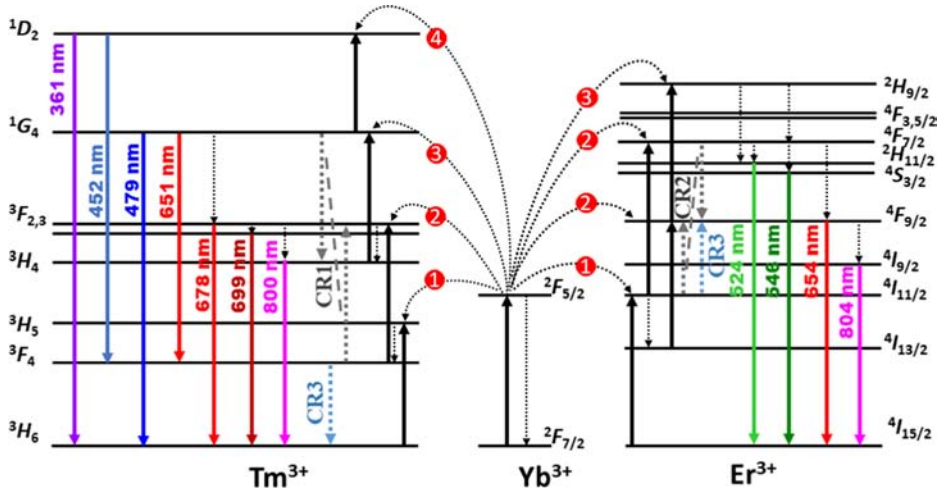

Figure 5. Schematic illustration of the energy transfer mechanism in Tm^{3+}, Er^{3+}-doped α-$NaYbF_4$ UCNPs.

which are almost in accordance with the results in Figure 4c. On the other hand, the *n* values in Figure 7b corresponding to the characteristic UCL of Er^{3+} ions (525, 544, and 658 nm) are 2.50, 2.47, and 2.63, respectively, indicating that both green and red upconversion emissions originate from the three-photon process of the Yb^{3+} ions when co-doping with the Tm^{3+} ions, and show an obvious difference compared with the previous *n* values in Er^{3+} monodoped α-$NaYbF_4$ (in Figure 4d), which may be ascribed to the ET process from Tm^{3+} to Er^{3+} ions. Moreover, the fluorescence decay curves of UCNPs have been investigated to further demonstrate the ET process between Tm^{3+} and Er^{3+} ions. Figure 7c shows the decay curves of NIR emission at 804 nm (Tm^{3+}: $^3H_4 \rightarrow {}^3H_6$ transition); the lifetime of Tm^{3+} ($^3H_4$) obtained from $NaYbF_4$:0.5%Tm^{3+}, 1%

DOI: 10.1021/acsomega.8b02936
ACS Omega 2018, 3, 17814−17820

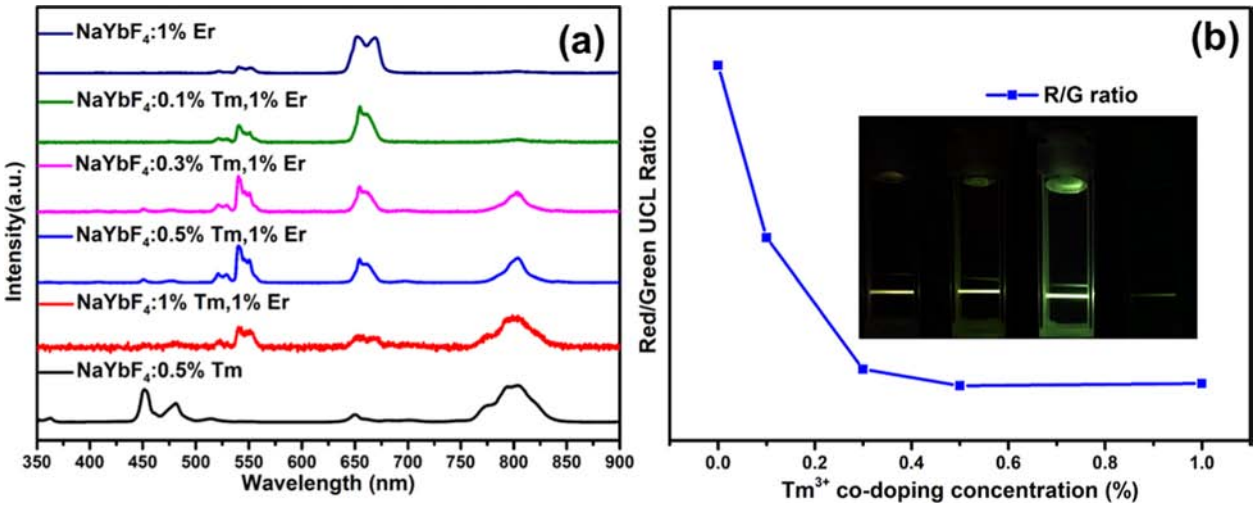

Figure 6. (a) Calibrated UCL spectra of different Tm^{3+}/Er^{3+}-doped $NaYbF_4$ samples under 980 nm laser excitation. (b) Red and green UCL ratio of the different Tm^{3+}/Er^{3+}-doped $NaYbF_4$ samples. The inset shows the visible photoluminescence of different Tm^{3+}/Er^{3+}-doped $NaYbF_4$ colloidal suspensions excited by a 980 nm laser.

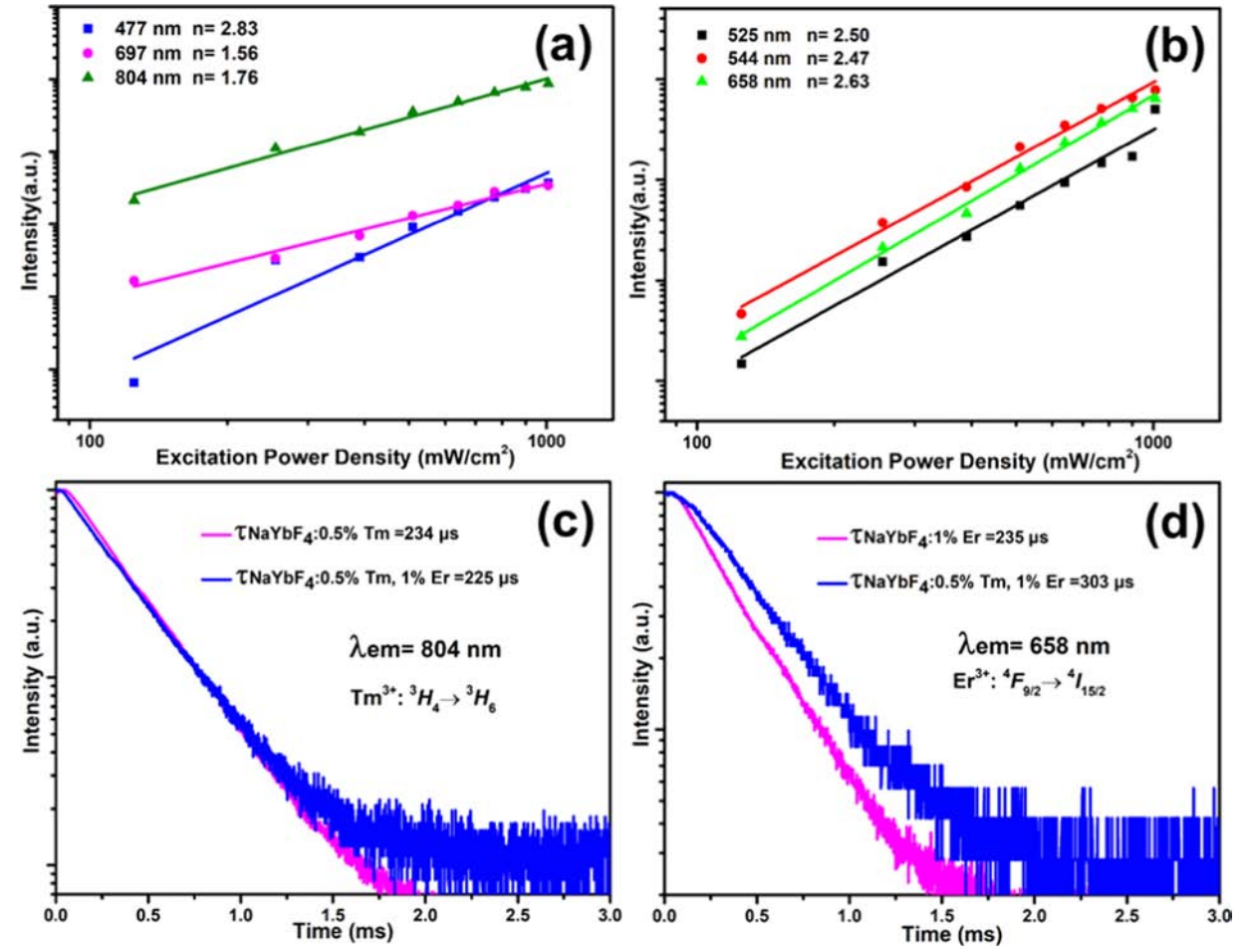

Figure 7. (a, b) Corresponding excitation power densities' dependence on the emission of $NaYbF_4$:0.5%Tm^{3+}, 1%Er^{3+} under 980 nm laser excitation. (c) Fluorescence decay curves of Tm^{3+} emission at 804 nm ($^3H_4 \rightarrow {}^3H_6$) from $NaYbF_4$:0.5%Tm^{3+} and $NaYbF_4$:0.5%Tm^{3+}, 1%Er^{3+} under 980 nm laser excitation. (d) Fluorescence decay curves of Er^{3+} emission at 658 nm ($^4F_{9/2} \rightarrow {}^4I_{15/2}$) from $NaYbF_4$:1%Er^{3+} and $NaYbF_4$:0.5% Tm^{3+}, 1%Er^{3+} under 980 nm laser excitation.

Er^{3+} (225 μs) presents a slight decrease compared with that from $NaYbF_4$:0.5%Tm^{3+} (234 μs). On the other hand, the lifetime of Er^{3+}: $^4F_{9/2} \rightarrow {}^4I_{15/2}$ at 658 nm in Figure 7d shows an obvious increase in $NaYbF_4$:0.5%Tm^{3+}, 1%Er^{3+} (234 μs) compared with that in $NaYbF_4$:1%Er^{3+} (303 μs). Therefore, with Tm^{3+} and Er^{3+} co-doping in α-$NaYbF_4$, besides their ET

DOI: 10.1021/acsomega.8b02936
ACS Omega 2018, 3, 17814−17820

process with the sensitizer Yb^{3+} ions, the nearly resonant cross-relaxation energy transfer process (CR3 process: $^3F_4$ (Tm^{3+}) + $^4I_{11/2}$ (Er^{3+}) → $^3H_6$ (Tm^{3+}) + $^4F_{9/2}$ (Er^{3+})) in Figure 5 probably occurs between the Tm^{3+} and Er^{3+} two dopants because the energy of the $^3F_4$→ $^3H_6$ transition matches that of the $^4I_{11/2}$ → $^4F_{9/2}$ transition.[14] In this way, the depopulation of Tm^{3+}: $^3F_4$ state might have a negative influence on the population on the upper level of Tm^{3+} (including the $^3H_4$ and $^1D_2$ states), leading to lifetime decrease of the Tm^{3+}: $^3H_4$ state. However, the CR3 process could not only facilitate the photon populated on the $^4F_{9/2}$ (Er^{3+}) state but also be conducive to the Yb-assisted three-photon ET process to the upper level: $^2H_{9/2}$ (Er^{3+}) state. Therefore, the green UCL emissions would be enhanced with the nonradiative transition from $^2H_{9/2}$ (Er^{3+}) to the lower level ($^4F_{7/2}$, $^2H_{11/2}$, $^4S_{3/2}$), as the results in Figure 6a depict.

2.3. In Vitro Cytotoxicity Test. Cytotoxicity test of the as-synthesized UCNPs in cells is a fundamental procedure to assess the potential biosecurity of UCNPs. Herein, the cytotoxicity of UCNPs with different concentrations (200–1000 μg/mL) was assessed by (3-(4,5-dimethylthiazol-2-yl)-2,5-diphenyltetrazolium bromide) (MTT) assay based on HeLa cells, as shown in Figure 8. After 24 h culture, the cellular

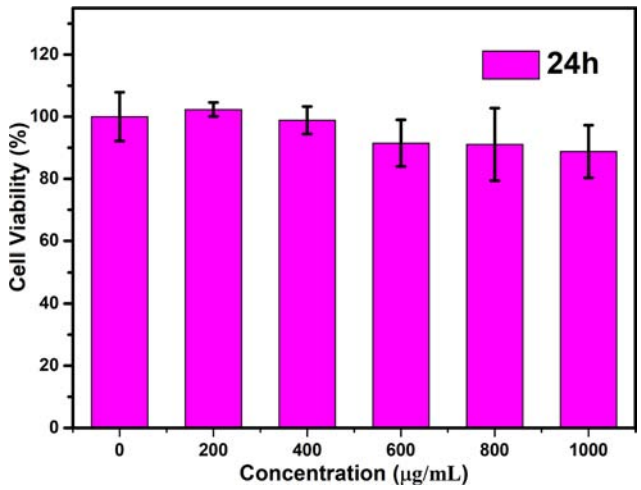

Figure 8. In vitro cytotoxicity of water-dispersible α-$NaYbF_4$ UCNPs against HeLa cells after 24 h incubation.

viability of the HeLa cells decreased to 89% at a concentration of 1000 μg/mL UCNPs in comparison to the control group, revealing that the UCNPs present low cytotoxicity and good biocompatibility for the potential biological applications.

3. CONCLUSIONS

In conclusion, Tm^{3+}/Er^{3+}-doped and -co-doped α-$NaYbF_4$ UCNPs with the average size of ∼13 nm were obtained via a mild hydrothermal method. The UCNPs exhibited strong blue and red UCL by doping Tm^{3+}, Er^{3+} under excitation of a 980 nm laser. The possible ET mechanism among Yb^{3+}/Tm^{3+}/Er^{3+} in α-$NaYbF_4$ UCNPs has been proposed on the basis of the plots of excitation power density and UCL spectra and the lifetime decay curves. Moreover, with the Tm^{3+} and Er^{3+} co-doping, short-wavelength UCL of Tm^{3+} ions quenched, whereas green UCL of Er^{3+} ion enhanced greatly, the R/G ratio in the UCL tends to be smaller as the doped Tm^{3+} ions increase, and controllable UCL can be tuned in the co-doped $NaYbF_4$:Er^{3+} UCNPs for the cross-relaxation ET from Tm^{3+} to Er^{3+}. Furthermore, the cell toxicity test results presented relatively low cytotoxicity in water-dispersible α-$NaYbF_4$. The Tm^{3+}, Er^{3+}-doped and -co-doped α-$NaYbF_4$ UCNPs possess many advantageous features including facile synthesis, controllable emission, and low cytotoxicity, which make them highly promising for applications in bioimaging and anticounterfeiting.

4. EXPERIMENTS

All of the rare-earth nitrates $RE(NO_3)_3$ (RE^{3+} = Yb^{3+}, Tm^{3+}, and Er^{3+}) (99.99% purity) were purchased from Alfa Aesar. Other chemicals were of analytical grade and used as received without further purification. All of the ion doping concentrations are in molar ratio in our experiments.

4.1. UCNPs' Synthesis. The doped α-$NaYbF_4$ nanocrystals were synthesized via a mild hydrothermal method with oleic acid as a stabilizing agent.[23,24] Typically, under magnetic stirring, 16 mL of ethanol was added into the aqueous solution with 2.4 g of NaOH and 4 mL of deionized water. Then, 40 mL of oleic acid was slowly added into the homogeneous solution with a vigorous magnetic stirring for 40 min. When forming a metal–oleic acid complex, 2 mmol stoichiometrically mixed $RE(NO_3)_3$ (RE^{3+} = Yb^{3+}, Tm^{3+}, Er^{3+}; Yb^{3+}/Tm^{3+}/Er^{3+} = $(1 - x - y)$:x:y. For example, α-$NaYbF_4$:1%Tm^{3+}, 1%Er^{3+}—Yb^{3+}/Tm^{3+}/Er^{3+} = 0.98:0.01:0.01) solution and 16 mL of an aqueous solution of NaF (1.0 mol/L) were added into the complex under magnetic stirring for another 20 min; the above-mentioned solution was then transferred into a 100 mL stainless-steel Teflon autoclave, and then sealed and heated at 120 °C for 12 h. After the autoclave was naturally cooled down to room temperature, the resulting precipitate was collected by centrifugation using a rotator speed of 10 000 rpm for 6 min, washed several times with deionized water and ethanol to remove oleic acid and other residual solvents, and finally redispersed in cyclohexane.

4.2. Characterization. The crystalline structures of nanocrystals were characterized by X-ray diffraction (XRD) in a D8 advance X-ray diffractometer (Bruker, Switzerland) at a scanning rate of 0.2°/min with Cu Kα radiation (151.54056 Å). The morphologies, size distributions, and compositions of as-prepared nanocrystals were investigated by field emission scanning electron microscopy (FE-SEM, Merlin, Zeiss) with an energy-dispersive X-ray spectrometer (EDS) and high-resolution transmission electron microscopy (HRTEM, Talos F200X, FEI). The upconversion emission spectra were recorded by a spectrophotometer (Ocean Optics) under the excitation of a 980 nm laser (BWT Beijing Ltd.). The photographic images were taken from the $NaYbF_4$:Tm^{3+}/Er^{3+} colloidal solutions dispersed in cyclohexane under the 980 nm laser excitation. Fluorescence lifetime was measured with an Andor spectrometer equipped with a MDO3034 digital oscilloscope (Tektronix) under the same laser excitation. All of the measurements were conducted at room temperature.

4.3. In Vitro Cytotoxicity. The water-dispersible α-$NaYbF_4$ nanocrystals were obtained via a typical acid-treatment process as previously reported.[25] For the cell cytotoxicity test, HeLa cells (5000 cells per well) were successfully seeded in a 96-well plate with Dulbecco's modified Eagle's medium and incubated overnight. Then, different concentrations of α-$NaYbF_4$ (0, 200, 400, 600, 800, and 1000 μg/mL) were added to each culture well. After further incubation for 24 h at 37 °C with 5% CO_2, 10 μL of (3-(4,5-dimethylthiazol-2-yl)-2,5-

DOI: 10.1021/acsomega.8b02936
ACS Omega 2018, 3, 17814–17820

diphenyltetrazolium bromide) (MTT) solution (5 mg/mL) was added into each well. The plates were incubated for another 4 h before replacing the original culture medium with 100 μL of dimethyl sulfoxide. The absorbance was measured at 490 nm, and the cell viability of HeLa cells was calculated as the ratio of the absorbance of the sample well to that of the control well measured by a microplate reader.

AUTHOR INFORMATION

Corresponding Author

*E-mail: yjliu@sustc.edu.cn.

ORCID

Yan Jun Liu: 0000-0001-8724-0434

Notes

The authors declare no competing financial interest.

ACKNOWLEDGMENTS

We acknowledge the financial support from the National Natural Science Foundation of China (Grant No. 61805113), Natural Science Foundation of Guangdong Province (Grant Nos 2017A030313034 and 2018A030310224), Shenzhen Science and Technology Innovation Commission (Grant Nos JCYJ20170817111349280 and KQTD2016030111203005), and Guangdong Innovative and Entrepreneurial Research Team Program (Grant No. 2017ZT07C071).

REFERENCES

(1) Wang, F.; Han, Y.; Lim, C.; Lu, Y.; Wang, J.; Xu, J.; Chen, H.; Zhang, C.; Hong, M.; Liu, X. Simultaneous phase and size control of upconversion nanocrystals through lanthanide doping. *Nature* **2010**, *463*, 1061−1065.

(2) Haase, M.; Schäfer, H. Upconverting nanoparticles. *Angew. Chem., Int. Ed.* **2011**, *50*, 5808−5829.

(3) Li, X.; Zhang, F.; Zhao, D. Lab on upconversion nanoparticles: optical properties and applications engineering via designed nanostructure. *Chem. Soc. Rev.* **2015**, *44*, 1346−1378.

(4) Zheng, W.; Huang, P.; Tu, D.; Ma, E.; Zhua, H.; Chen, X. Lanthanide-doped upconversion nano-bioprobes: electronic structures, optical properties, and biodetection. *Chem. Soc. Rev.* **2015**, *44*, 1379−1415.

(5) Zhao, J.; Jin, D.; Schartner, E. P.; Lu, Y.; Liu, Y.; Zvyagin, A. V.; Zhang, L.; Dawes, J. M.; Xi, P.; Piper, J. A.; Goldys, E. M.; Monro, T. M. Single-nanocrystal sensitivity achieved by enhanced upconversion luminescence. *Nat. Nanotechnol.* **2013**, *8*, 729−734.

(6) Zhou, B.; Shi, B.; Jin, D.; Liu, X. Controlling upconversion nanocrystals for emerging applications. *Nat. Nanotechnol.* **2015**, *10*, 924−936.

(7) Krämer, K. W.; Biner, D.; Frei, G.; Güdel, H. U.; Hehlen, M. P.; Lüthi, S. R. Hexagonal sodium yttrium fluoride based green and blue emitting upconversion phosphors. *Chem. Mater.* **2004**, *16*, 1244−1251.

(8) Wang, J.; Deng, R.; MacDonald, M. A.; Chen, B.; Yuan, J.; Wang, F.; Chi, D.; Hor, T. S. A.; Zhang, P.; Liu, G.; Han, Y.; Liu, X. Enhancing multiphoton upconversion through energy clustering at sublattice level. *Nat. Mat.* **2014**, *13*, 157−162.

(9) Chen, X.; Jin, L.; Kong, W.; Sun, T.; Zhang, W.; Liu, X.; Fan, J.; Yu, S.; Wang, F. Confining energy migration in upconversion nanoparticles towards deep ultraviolet lasing. *Nat. Commun.* **2016**, *7*, No. 10304.

(10) Shen, J.; Chen, G.; Ohulchanskyy, T. Y.; Kesseli, S. J.; Buchholz, S.; Li, Z.; Prasad, P. N.; Han, G. Tunable near infrared to ultraviolet upconversion luminescence enhancement in (α-$NaYF_4$:Yb,Tm)/CaF_2 core/shell nanoparticles for in situ real-time recorded biocompatible photoactivation. *Small* **2013**, *9*, 3212.

(11) Chen, G.; Ohulchanskyy, T. Y.; Kumar, R.; Ågren, H.; Prasad, P. N. Ultrasmall monodisperse $NaYF_4$:Yb^{3+}/Tm^{3+} nanocrystals with enhanced near-infrared to near-Infrared upconversion photoluminescence. *ACS Nano* **2010**, *4*, 3163−3168.

(12) Chen, G.; Shen, J.; Ohulchanskyy, T. Y.; Patel, N. J.; Kutikov, A.; Li, Z.; Song, J.; Pandey, R. K.; Agren, H.; Prasad, P. N.; Han, G. (α-$NaYbF_4$:Tm^{3+})/CaF_2 core/Shell nanoparticles with efficient near-infrared to near-infrared upconversion for high-contrast deep tissue bioimaging. *ACS Nano* **2012**, *6*, 8280−8287.

(13) Dong, H.; Sun, L.; Yan, C. Energy transfer in lanthanide upconversion studies for extended optical applications. *Chem. Soc. Rev.* **2015**, *44*, 1608−1634.

(14) Chan, E. M.; Han, G.; Goldberg, J. D.; Gargas, D. J.; Ostrowski, A. D.; Schuck, P. J.; Cohen, B. E.; Milliron, D. J. Combinatorial discovery of lanthanide-doped nanocrystals with spectrally pure upconverted emission. *Nano Lett.* **2012**, *12*, 3839−3845.

(15) Wang, F.; Liu, X. Upconversion multicolor fine-tuning: Visible to near-infrared emission from lanthanide-doped $NaYF_4$ nanoparticles. *J. Am. Chem. Soc.* **2008**, *130*, 5642−5643.

(16) Niu, N.; Yang, P.; He, F.; Zhang, X.; Gai, S.; Li, C.; Lin, J. Tunable multicolor and bright white emission of one-dimensional $NaLuF_4$:Yb^{3+}, Ln^{3+} (Ln = Er, Tm, Ho, Er/Tm, Tm/Ho) microstructures. *J. Mater. Chem.* **2012**, *22*, 10889−10899.

(17) Yang, J.; Zhang, C.; Peng, C.; Li, C.; Wang, L.; Chai, R.; Lin, J. Controllable red, green, blue (RGB) and bright white upconversion luminescence of Lu_2O_3: Yb^{3+}/Er^{3+}/Tm^{3+} nanocrystals through single laser excitation at 980 nm. *Chem. - Eur. J.* **2009**, *15*, 4649−4655.

(18) Liu, X.; Wang, Y.; Li, X.; Yi, Z.; Deng, R.; Liang, L.; Xie, X.; Loong, D. T. B.; Song, S.; Fan, D.; All, A. H.; Zhang, H. J.; Huang, L.; Liu, X. Binary temporal upconversion codes of Mn^{2+}-activated nanoparticles for multilevel anti-counterfeiting. *Nat. Commun.* **2017**, *8*, No. 899.

(19) Lei, L.; Chen, D.; Li, C.; Huang, F.; Zhang, J.; Xu, S. Inverse thermal quenching effect in lanthanide-doped upconversion nanocrystals for anti-counterfeiting. *J. Mater. Chem. C* **2018**, *6*, 5427−5433.

(20) Lei, L.; Xia, J.; Cheng, Y.; Wang, Y.; Bai, G.; Xia, H.; Xu, S. Enhancing negative thermal quenching effect via low-valence doping in two-dimensional confined core−shell upconversion nanocrystals. *J. Mater. Chem. C* **2018**, 11587.

(21) Pollnau, M.; Gamelin, D. R.; Lüthi, S. R.; Güdel, H. U.; Hehlen, M. P. Power dependence of upconversion luminescence in lanthanide and transition-metal-ion systems. *Phys. Rev. B: Condens. Matter Mater. Phys.* **2000**, *61*, 3337−3346.

(22) Xue, M.; Zhu, X.; Qiu, X.; Gu, Y.; Feng, W.; Li, F. Highly enhanced cooperative upconversion luminescence through energy transfer optimization and quenching protection. *ACS Appl. Mater. Interfaces* **2016**, *8*, 17894−17901.

(23) Wang, X.; Zhuang, J.; Peng, Q.; Li, Y. A general strategy for nanocrystal synthesis. *Nature* **2005**, *437*, 121−124.

(24) Zeng, S.; Ren, G.; Xu, C.; Yang, Q. High uniformity and monodispersity of sodium rare-earth fluoride nanocrystals: controllable synthesis, shape evolution and optical properties. *CrystEngComm* **2011**, *13*, 1384−1390.

(25) Bogdan, N.; Vetrone, F.; Ozin, G. A.; Capobianco, J. A. Synthesis of ligand-free colloidally stable water dispersible brightly luminescent lanthanide-doped upconverting nanoparticles. *Nano Lett.* **2011**, *11*, 835−840.

DOI: 10.1021/acsomega.8b02936
ACS Omega 2018, 3, 17814−17820